การศึกษาแบบจำลองเชิงโมเลกุลของการดูดซับสารอะโรมาติกไฮโดรคาร์บอน
แบบไม่มีขั้วและมีขั้วบนพื้นผิวกราไฟท์

นายพิษณุ   สุขนิยม   รหัส 54360452

นายวุฒิชัย   ชัยยอด   รหัส 54360506

ปริญญานิพนธ์นี้เป็นส่วนหนึ่งของการศึกษาหลักสูตรปริญญาวิศวกรรมศาสตรบัณฑิต

สาขาวิชาวิศวกรรมเคมี ภาควิชาวิศวกรรมอุตสาหการ

คณะวิศวกรรมศาสตร์ มหาวิทยาลัยนเรศวร

ปีการศึกษา 2557

ใบรับรองปริญญานิพนธ์

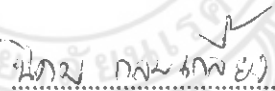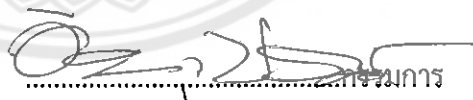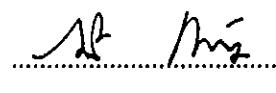|	
ชื่อหัวข้อโครงงาน	การศึกษาแบบจำลองเชิงโมเลกุลของการดูดซับสารอะโรมาติก
	ไฮโดรคาร์บอนแบบมีไม่มีขั้วและมีขั้วบนพื้นผิวกราไฟต์
ผู้ดำเนินโครงการ	นายพิษณุ สุขนิยม รหัส 54360452
	นายวุฒิชัย ชัยยอด รหัส 54360506
ที่ปรึกษาโครงงาน	ดร.นิคม กลมเกลี้ยง
สาขาวิชา	วิศวกรรมเคมี
ภาควิชา	วิศวกรรมอุตสาหการ
ปีการศึกษา	2557

....
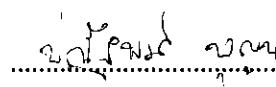
คณะวิศวกรรมศาสตร์ มหาวิทยาลัยนเรศวร อนุมัติให้ปริญญานิพนธ์ฉบับนี้เป็นส่วนหนึ่งของ
การศึกษาตามหลักสูตรวิศวกรรมศาสตรบัณฑิต สาขาวิชาวิศวกรรมเคมี

....ที่ปรึกษาโครงงาน
(ดร.นิคม กลมเกลี้ยง)

....กรรมการ
(ดร.อิศราวุธ ประเสริฐสังข์)

....กรรมการ
(รองศาสตราจารย์ ดร.สมร หิรัญประดิษฐกุล)

....กรรมการ
(ดร.ปณัฐพงศ์ บุญนวล)

ชื่อหัวข้อโครงงาน	การศึกษาแบบจำลองเชิงโมเลกุลของการดูดซับสารอะโรมาติก ไฮโดรคาร์บอนแบบมีไม่มีขั้วและมีขั้วบนพื้นผิวกราไฟต์		
ผู้ดำเนินโครงการ	นายพิษณุ	สุขนิยม	รหัส 54360452
	นายวุฒิชัย	ชัยยอด	รหัส 54360506
ที่ปรึกษาโครงงาน	ดร.นิคม	กลมเกลี้ยง	
สาขาวิชา	วิศวกรรมเคมี		
ภาควิชา	วิศวกรรมอุตสาหการ		
ปีการศึกษา	2557		

บทคัดย่อ

แบบจำลอง Grand canonical Monte Carlo ถูกใช้ในการศึกษาการดูดซับทั้ง การดูดซับที่อุณหภูมิคงที่ และความร้อนของการดูดซับ ของสารประกอบอะโรมาติกไฮโดรคาร์บอน ทั้งที่ไม่มีขั้วและมีขั้ว บนพื้นผิวของกราไฟท์ ซึ่งเราได้พิจารณาทั้งขนาดและรูปทรงของสารประกอบอะโรมาติกไฮโดรคาร์บอนที่ไม่มีขั้วเช่น เบนซีนโทลูอีน และ ไซลีน แต่ในขณะที่ ไพริดีนเป็นสารประกอบอะโรมาติกไฮโดรคาร์บอนที่มีขั้ว และมีรูปร่างคล้ายเบนซีน จึงได้ทำการเปรียบเทียบกันพบว่าการก่อตัวของโครงสร้าง เบนซีนโทลูอีน และ ไซลีน นั้นไม่ต่างกับ ไพริดีน ซึ่งทั้งสามสารที่ไม่มีขั้วนั้นมีการจัดเรียงโมเลกุลทั้งแบบขนานและแบบเอียงมากน้อยแตกต่างกันไปโดย เบนซีน<โทลูอีน< ไซลีน และ เบนซีน>โทลูอีน>ไซลีน ตามลำดับ ในการก่อตัวของ เบนซีนโทลูอีน และ ไซลีน ในชั้นการดูดซับแรกนั้นมีตำแหน่งการการก่อตัวใกล้พื้นผิวมากกว่าไพริดีน แต่ในชั้นการดูดซับที่สองการก่อตัวของไพริดีนนั้นใกล้พื้นผิวกว่าเล็กน้อย เป็นน่าสนใจว่าพีครองของไพริดีนในชั้นการดูดซับพบว่าไพริดีนนั้นมีการฟอร์มตัวโดยให้อะตอมของไนโตรเจนอยู่ห่างจากพื้นผิว

Title	Molecular Simulation study of Adsorption of non-polar and polar aromatic hydrocarbons on a Graphite surface.
Author	PhitsanuSukniyom
	VutichaiChaiyot
Advisor	Dr.NikomKlomkliang, Ph.D.
Academic Paper	Thesis B.Eng. in Chemical Engineering,
	Naresuan University, 2015
Keywords	Polar fluids, Adsorption, Isosteric heat, Graphite surface,
	Molecular simulation

....

ABSTRACT

Grand canonical Monte Carlo simulation has been carried out to investigate the adsorption isothrem and isosteric heat of non-polar and polar aromatic hydrocarbons on graphite surface. We consider difference of the site and curvature of non-polar aromatic hydrocarbons such as benzene, toluene and xylene (BTX) while pyridine is taken as a polar aromatic hydrocarbon to compare with the same curvature as benzene. It has been found that the structure formations of BTX are not different exception of the amount of molecule having parallel and slant formations on the surface as in order of B<T<X and B>T>X, respectively. The structure formations of pyridine are similar to that of BTX, only the position of the parallel configuration from the surface of pyridine is slightly higher but the second layer is slightly lower. Interestingly, the minor peak of the first layer of pyridine is due to the N atom of pyridine is far away from the surface.

ACKNOWLEDGEMENTS

LIST OF CONTENTS

LIST OF TABLES

Table	**Page**

LIST OF FIGURES

LIST OF FIGURES (CONT.)

CHAPTER I

INTRODUCTION AND LITERATURE REVIEW

1.1 Significance of the Problem

Aromatic hydrocarbons such as benzene, toluene, xylene, and pyridine are hazardous organic compounds that are emitted from chemical and petrochemical industries. It has been reported that these aromatic hydrocarbons are neurotoxic, and consequently cause diseases of the nervous system and sterility [1]. Stricter environmental regulations require that aromatics must be removed before the effluents can be safely discharged into the environment. Among the various technologies that are available, adsorption is the simplest means to achieve this goal with activated carbon (AC), silica gel, and zeolite being the possible candidates as adsorbents. Among them, AC is preferred because of its non-polar surface and high surface area [2, 3].

The physisorption of aromatics on a graphitic surface has been studied thoroughly both experimentally [4-15] and theoretically [16-20]; the affinity for the adsorbent being the most important criterion for better design of an adsorption system. For example AC, [3, 21] carbon nanotubes [22, 23], and advanced adsorbents with hexagonal pores [24-26] have all been the subject of investigation in the last decade.

1.2 Literature review

In recent years, with the advances of the computer simulation, molecular simulation has also been used to study benzene adsorption on graphite. Vernov and Steele [16, 17] used Monte Carlo simulation to investigate the structures and energies of benzene adsorption on graphite at 85 and 298K. They found that the heat of adsorption was nearly constant in the sub-monolayer region, in agreement with the calorimetric data of Isirikyan and Kiselev [6]. This constant heat is attributed to cancellation between the increase in the benzene-benzene interaction and the decrease in the benzene-adsorbent interaction; which changes as the orientation of benzene molecules changes with increased loading in the sub-monolayer region. The structure

of the second layer was found to be less ordered than that of the first layer, as a result of the weaker interactions of the benzene molecules in the second layer. Matties and Hentschke [18, 19] used molecular dynamics to study the structure of the benzene adsorbate in the first and higher layers on the basal plane of graphite over a wide range of temperature (60–320K). Their results showed that ordering beyond the nearest neighbours decreases rapidly with coverage, and is virtually non-existent for second and higher layers. However, since molecular dynamics does not yield adsorption isotherms or heats their simulation results cannot be tested against experimental data. More detailed study of isotherms, heats and the structure of adsorbed benzene on graphite using grand canonical Monte Carlo (GCMC) simulation was presented by Do and Do [20]. They investigated the performance of various potential models for benzene that were available up to 2006, the united atom models TraPPE-UA-6 [27] and TraPPE-UA-9 [28] and the all atom model OPLS-AA (with 12 dispersive sites and 12 partial charges) [29], for their suitability in correctly describing the experimental adsorption isotherm and the heat of adsorption, and found that the TraPPE-UA-9 gave the better results. From the simulation data, they found that at very low loadings, most benzene molecules adopt an orientation parallel to the surface which is the most energetically favourable position. When the loading is increased within the sub-monolayer coverage, some benzene molecules adopt a slant configuration, due to the quadrupolar interactions between benzene molecules. However, the work by Do and Do was restricted to the sub-monolayer region, and therefore a molecular simulation of benzene adsorption on GTCB beyond the first layer is desirable to assess the ability of the potential models to describe the isotherm and isosteric heat and to explore how molecules in higher layers affect the orientation of molecules in the first layer. Furthermore, a new potential model was recently proposed by Rai and Siepmann [30], TraPPE-EH, which includes twelve dispersive sites (carbon and hydrogen atoms) and twelve partial charges on these atoms, and it is of interest to test its capability to describe benzene adsorption. These authors compared this new model with previous potential models for benzene, and have found that this model and OPLS-AA are significantly more accurate than the 6-site model (TraPPE-UA-6) and the 9-site model (TraPPE-UA-9) for the description of vapour-liquid equilibria at 298.15K. The OPLS-AA model performed well at 298.15K (where

it was fitted) but its performance degraded rapidly with increasing temperature. Interestingly the better models are the ones that account explicitly for the hydrogen atoms.

The affinity of the adsorbent for the adsorbate is characterized by the Henry constant, and has been obtained experimentally for BTX in a number of carbonaceous systems at various temperatures [4, 6, 7, 12, 13, 31]. These authors have shown that the order of affinity is B < T < X, due to the methyl groups attached to the benzene ring that augment the interaction with the surface. Although xylene is the strongest adsorbate on this basis, there are conflicting reports in the literature that the adsorption capacity for benzene is the highest (among BTX) in some activated carbons [2, 3, 32] but is the lowest in others [21]. This raises questions about the affinity and packing of BTX in a confined space. Although it has been reported that the surface functional group can have an effect on the packing [33] we concentrate our investigation on the effects of the confined space, in terms of its size, curvature, and polar site on the packing of BTX and pyridine using a grand canonical Monte Carlo (GCMC) simulation. Simulation of BTX adsorption on a graphite surface has been studied previously [34, 35]. On the other hand, there are no reports in the literature of simulation of pyridine adsorption on a graphite surface, and we therefore study its adsorption on a planar graphite surface first to compare with that of non-polar aromatic hydrocarbons.

1.3 Research Objectives

The main work for this research is to study physics of adsorption for aromatic hydrocarbon. Which concentrate the adsorption isotherm and heat of adsorption of pyridine to compare with experiment data. And predict the adsorption of pyridine at 273K and 323K of temperature.

1. To study adsorption isotherm and heat of adsorption for aromatic hydrocarbon.

2. To study of packing for non-polar and polar aromatic hydrocarbon.

3. To compare results of simulation for aromatic hydrocarbons with experimental data.

1.4 Scope

In this research require to study the adsorption of pyridine on GTCB. We divide our works into three parts. In the first, we require to study the adsorption isotherm of pyridine on graphite surface at ambient temperature. In the second part, we require to study the heats of adsorption of pyridine on graphite surface at ambient temperature. Third part we require to study affinity and packing of pyridine on graphite surface. All of three part we use Grand Canonical Monte Carlo simulation to compare the simulation results and experimental data at 293K. For prediction the adsorption of pyridine at other temperature we choose 273K to 323K.

1.5 Outcomes

This research will understand fundamental adsorption of aromatic hydrocarbons on graphitized surface. The adsorption on surface in microscale is not advised in experiment but can be seen by GCMC. This study will provide fundamental adsorption for the design to industrial for manage the toxic fluids not only aromatic hydrocarbons or amount of adsorbent needed and including heat form the exothermic system.

CHAPTER II

THEORY AND METHODOLOGY

2.1 Adsorbate

Adsorbates in this work have non-polar and polar aromatic hydrocarbons. The physical properties have been shown in Table 2.1 and common structure of adsorbates have been shown in Figure 2.1

Table 2.1 Physical properties for BTX and Pyridine.

Properties	Benzene	Toluene	p-Xylene	Pyridine
Molecular formula	C_6H_6	C_7H_8	C_8H_{10}	C_5H_5N
Molar mass (g/mol)	78.11	92.14	106.17	79.10
Dipole moment (D)	0	0.36	0.07	2.20
Melting point (°C)	5.53	−95	13.2	−41.6
Boiling point (°C)	80.1	111	138.35	115.2
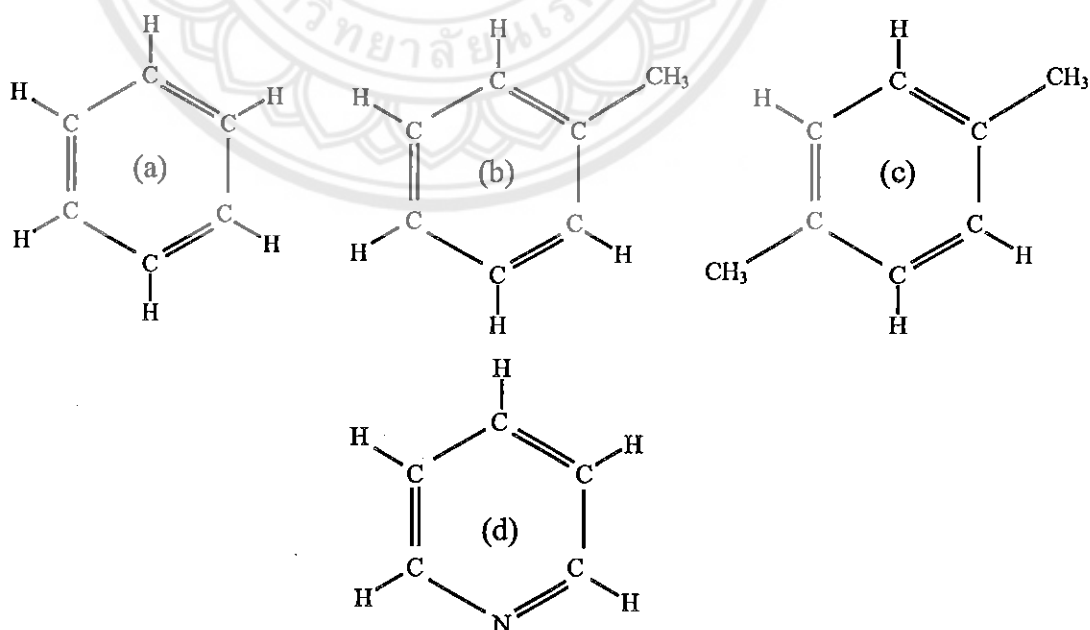
Figure 2.1 Structure of (a) Benzene, (b) Toluene, (c) Xylene, and (d) Pyridine.

2.2 Potential models

It has been found in our previous work [34] that the TraPPE-UA models [28] comprising six Lennard Jones (LJ) sites and three charged sites can describe the experimental data for fluid benzene reasonably well, and we will employ these models here. The six LJ sites are at the centres of the carbon atoms of the aromatic ring with a C(aro)–C(aro) bond length of 1.40Å. For toluene, additional dispersive sites are located at the centre of mass of the carbon atom of the methyl group and C(aro)–CH$_3$ bond length is 1.54Å. A positive partial charge (+2.42e) is placed at the centre of the benzene ring, and two negative partial charges (–1.21e each) on both sides of the ring are placed at a distance of 0.785Å normal to the ring to account for the quadrupole. The molecular parameters of non-polar aromatics are listed in Table 2.2. For polar aromatic, pyridine, the TraPPE-UA model is used [36] as listed in Table 2.3.

Table 2.2 Potential parameters for BTX.

Model	Group	σ (Å)	ε/k_B (K)	q (e)
TraPPE-UA	CH	3.74	48.00	
	C	3.88	21.00	
	CH$_3$	3.75	98.00	
	z = 0			+2.420
	z = ± 0.785 Å			–1.210
	Bound length			
	C(aro)-C(aro)		1.40Å	
	C(aro)-CH$_3$		1.54Å	

Table 2.3 Potential parameters for pyridine.

Model	Group	σ (Å)	ε/k_B (K)	q (e)
TraPPE-UA	(N)	3.45	28	-0.66
	(CH)-N	3.74	48	+0.33
	(CH)-CH	3.74	48	0
	Bound length			
	C(aro)-C(aro)		1.40Å	
	C(aro)-N		1.40Å	
	Angles			
	C(aro)-C(aro)-C(aro)		120°	
	C(aro)-C(aro)-N		120°	
	C(aro)-N-C(aro)		120°	

The commonly accepted single-site Lennard Jones (LJ) 12–6 and Steele 10–4–3 potential energy equations work well for small pseudo-spherical molecules. However, for large molecules, such as benzene, single-site models are not suitable. Here we consider benzene to be a hexagonal molecule composed of at least 6 sites. For a polyatomic molecule with M LJ site centres, the potential energy of interaction between a site a on a molecule i with a site b on a molecule j can be calculated using the following LJ 12–6 equation:

$$U_{i,j}^{(a,b)} = \sum_{a=1}^{M} \sum_{b=1}^{M} 4\varepsilon_{i,j}^{(a,b)} \left[\left(\frac{\sigma_{i,j}^{(a,b)}}{r_{i,j}^{(a,b)}} \right)^{12} - \left(\frac{\sigma_{i,j}^{(a,b)}}{r_{i,j}^{(a,b)}} \right)^{6} \right] \tag{2.1}$$

where $r_{i,j}^{(a,b)}$ is the separation distance between the LJ site a on molecule i and the LJ site b on molecule j, $\sigma_{i,j}^{(a,b)}$ and $\varepsilon_{i,j}^{(a,b)}$ are the cross collision diameter and the cross well-depth of the interaction energy, respectively. The cross parameters, $\sigma_{i,j}^{(a,b)}$ and $\varepsilon_{i,j}^{(a,b)}$ can be determined by the Lorentz–Berthelot mixing rules: $\sigma_{i,j}^{(a,b)} = (\sigma_{i,j}^{(a,a)} + \sigma_{i,j}^{(b,b)})/2$ and $\varepsilon_{i,j}^{(a,b)} = (\varepsilon_{i,j}^{(a,a)} \varepsilon_{i,j}^{(b,b)})^{1/2}$. The interaction energy due to the electrostatic force between a charge α on a molecule i and a charge β on a molecule j can be calculated from the Coulomb law of electrostatic interaction

$$U_{q;i,j}^{(\alpha,\beta)} = \sum_{\alpha=1}^{M_q} \sum_{\beta=1}^{M_q} \frac{1}{4\pi\varepsilon_0} \frac{q_i^\alpha q_j^\beta}{r_{i,j}^{(\alpha,\beta)}} \tag{2.2}$$

where M_q is the number of charges on the molecule, ε_0 is the permittivity of free space [$\varepsilon_0 = 10^7/(4\pi c^2) = 8.8543 \times 10^{-12}$ C^{2}J^{-1}m^{-1}, c is the speed of light], $r_{i,j}^{(\alpha,\beta)}$ is the distance between two charges α and β on molecules i and j, respectively, q_i^α is the value of charge α on molecule i, and q_j^β is the value of charge β on molecule j.

2.3 Adsorbate-adsorbent interaction energy

We have shown in earlier work [34] that at ambient temperature graphite can be effectively modelled as a structure-less solid, since simulation results from this model are practically the same as those from a discrete atom model. The potential energy between one adsorbate molecule and a graphite surface is calculated from the 10–4–3 Steele equation [37]:

$$U_{i,s} = \sum_{a=1}^{M} 4\pi\varepsilon_i^{(a,s)} \rho_s \left[\sigma_i^{(a,s)}\right]^2 \left[\frac{1}{5}\left(\frac{\sigma_i^{(a,s)}}{z_i^a}\right)^{10} - \frac{1}{2}\left(\frac{\sigma_i^{(a,s)}}{z_i^a}\right)^4 - \frac{\left[\sigma_i^{(a,s)}\right]^4}{6\Delta\left(z_i^a + 0.61\Delta\right)^3} \right] \tag{2.3}$$

where z_i^a is the distance of site a of molecule i from the graphite surface, $\varepsilon_i^{(a,s)}$ and $\sigma_i^{(a,s)}$ are the adsorptive-graphite interaction potential well-depth and intermolecular collision diameter respectively (estimated with the Lorentz-Berthelot mixing rule), ρ_s is the surface density (taken as 38.2nm^{-2} in this work), and Δ is the spacing between the two adjacent graphite layer (0.3354nm). In reference Klomkliang et al.[34] the well-depth of interaction energy for the adsorbate-adsorbent interaction was replaced by $\varepsilon'_{sf} = (1-k_{sf})\varepsilon_{sf}$, adjusted with the binary interaction parameter, k_{sf}, to give agreement between the experimental Henry constant and GCMC simulations. The molecular parameters for a carbon atom in the graphene layer are $\sigma_i^{(s)} = 3.4$Å and $\varepsilon_i^{(s)}/k_B = 28$K.

2.4 Methodology

Grand canonical Monte Carlo simulation

To model an open surface, we used a slit pore wide enough to behave as two independent surfaces. The box length was more than 10 times the collision diameter (80Å×80Å×80Å for open surface and the cut-off radius was half the box length. The standard Metropolis sampling scheme [38] was applied. The number of cycles for the equilibration and statistics collection steps was 50,000 each. In each cycle, there are 1,000 displacement moves (with rotation), and insertion and deletion trials with equal probability. The average surface excess for an open surface was calculated from

$$\Gamma_{av} = \frac{\langle N \rangle - \rho_b V_{acc}}{2A}$$
(2.4)

where ρ_b is the bulk molecular density, A is surface area of one wall of the simulation box, and $\langle N \rangle$ is the ensemble average of the number of particles in the pore. A thermodynamic quantity of interest that can be readily obtained from the GCMC simulations is the isosteric heat. Using the fluctuation theory, [39] it is calculated from [40]

$$q_{Isos} = \frac{\langle U \rangle \langle N \rangle - \langle UN \rangle}{\langle N^2 \rangle - \langle N \rangle \langle N \rangle} + k_B T$$
(2.5)

where $\langle \ \rangle$ is the ensemble average, N is the number of particles, and U is the configuration energy of the system.

In order to study the variation of density from the surface, the local density of the centre of benzene ring is defined as:

$$\rho(z) = \frac{\langle \Delta N_{z+\Delta z} \rangle}{L_x L_y \Delta z}$$
(2.6)

where $\langle \Delta N_{z+\Delta z} \rangle$ is the ensemble average of the number of molecules whose benzene ring centres are located in the segment.

CHAPTER III

RESULTS AND DISCUSSION

3.1 Non-polar aromatic hydrocarbons on graphitized surface

Adsorption on GTCB of non-polar aromatic hydrocarbons such as benzene, toluene and xylene has been studied in our previous work [35, 41], where reliable isotherms and isosteric heats can be found. Figures 3.1a and 3.1b show the adsorption isotherms and isosteric heats, respectively, at 293K of these adsorbates on GTCB obtained by our simulation with assumption of perfect graphite surface and experimental data from the literature [5, 6]. Although these patterns have been thoroughly described in the literature, we shall explain briefly here for the purpose of comparison with the extension work on polar aromatics such as pyridine and phenol presented in the next section.

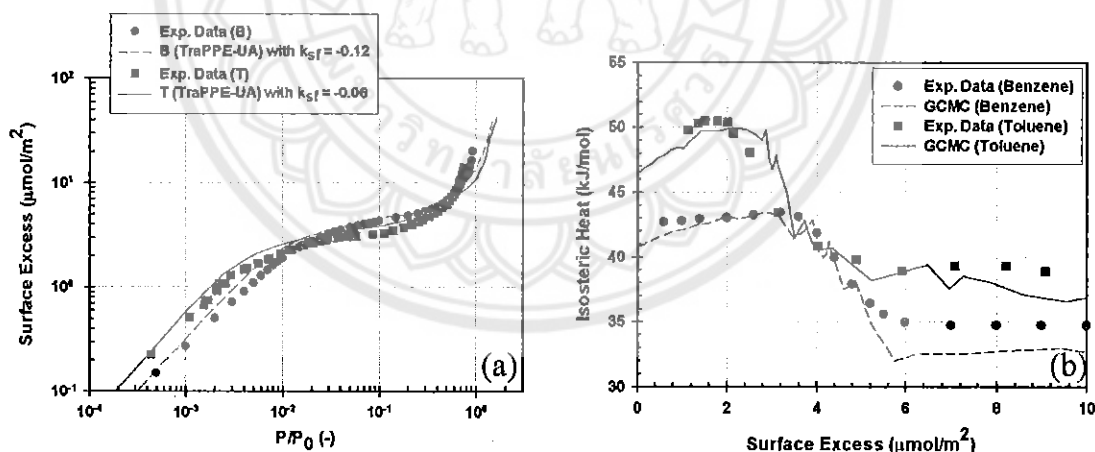Figure 3.1 (a) Adsorption isotherms and (b) isosteric heats of benzene and toluene on GTCB at 293K obtained with GCMC and experimental data from the literature [5, 6].

Good agreement between simulation and experiment can be achieved for loadings of $10\mu mol/m^2$ for benzene and $8\mu mol/m^2$ for toluene, when a binary interaction parameter k_{sf} of -0.12 and -0.06 was set for for benzene and toluene,

respectively. Unfortunately, the experimental data for xylene adsorption on a graphite surface are not available in the literature, we can only study xylene adsorption with molecular simulation. To compare the adsorption performance of BTX on a graphite surface with the same basis of potential models, we have therefore carried out simulations without introducing the binary interaction parameter.
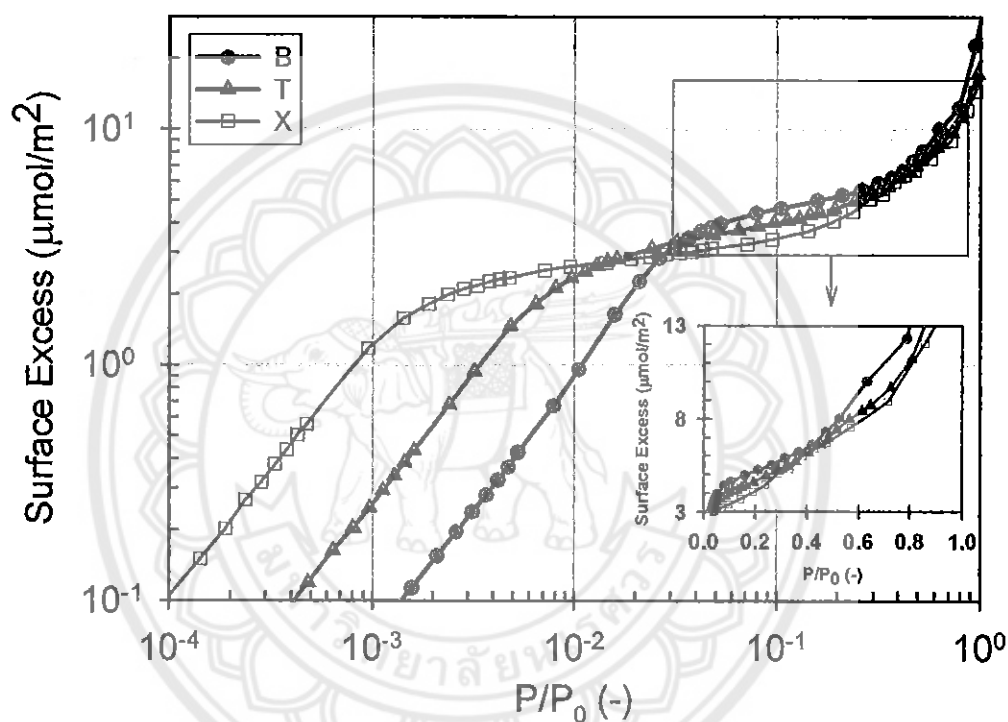
Figure 3.2 Adsorption isotherms of BTX on graphite surface at 298K obtained
from GCMC

Figure 3.2 shows the simulated isotherms of BTX adsorption on a graphite surface at 298K as surface excess (μmol/m^2) as a function of relative pressure, P/P_0. Since different adsorbates have different saturation vapour pressure and the driving force for adsorption is the reduced pressure, where P_0 is the simulated saturation vapour pressure (2, 6, and 20kPa, for benzene, toluene and xylene, respectively) [28]. It is seen that the order of the affinity towards the graphite surface is B < T < X, which is expected because of the stronger dispersion interaction from the additional methyl groups. Interestingly, the adsorptive capacity of benzene, expressed in mole per

surface area, becomes greater than those of the other two adsorbates. This result comes about because benzene has a smaller molar volume than the other two adsorptives.
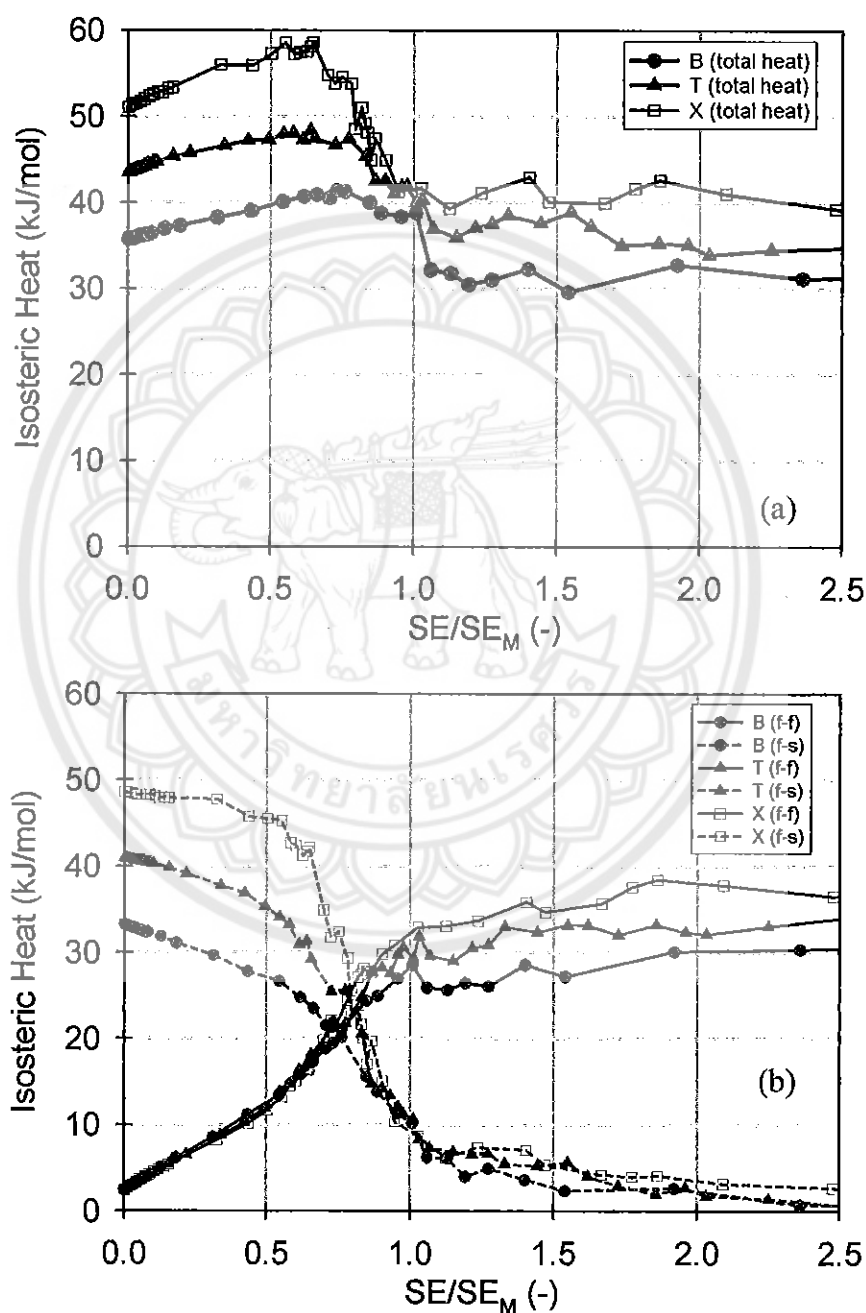

Figure 3.3 Isosteric heats of BTX on GTCB at 298K. (a) Total isosteric heat. (b) fluid-fluid and fluid-solid isosteric heats. SE is surface excess at any loadings. SE_M is monolayer coverage concentration.

The isosteric heat of BTX adsorption on a graphite surface at 298K is shown in Figure 3.3. At zero loading, the isosteric heats of benzene, toluene, and xylene are 36, 43, and 51kJ/mol, respectively, which is in agreement with the calorimetric data of Kiselev et al.[31], that the zero loading-isosteric heat is in the order B < T < X, and is consistent with the order of the Henry constant. The isosteric heat versus loading curve is typical of adsorbates that have stronger fluid-solid interaction compared to fluid-fluid interaction, and the order of heat at any loadings is the same as that at zero loading.

The local density distribution versus the distance from the surface to the centre of the benzene ring is shown in Figure 3.4 for BTX adsorption on a graphite surface. There are two overlapped peaks in the monolayer region; the main peak at 3.5Å corresponds to molecules parallel to the plane of the surface and a minor peak at 4.5Å corresponds to non-parallel configurations with their ring centres shifted further away from the surface to maximize the quadrupolar interaction between adsorbate molecules [34]. Interestingly the magnitude of the major and minor peaks is in order: B < T < X and B > T > X, respectively because the stronger interaction of the methyl groups with the surface acts against this trend.
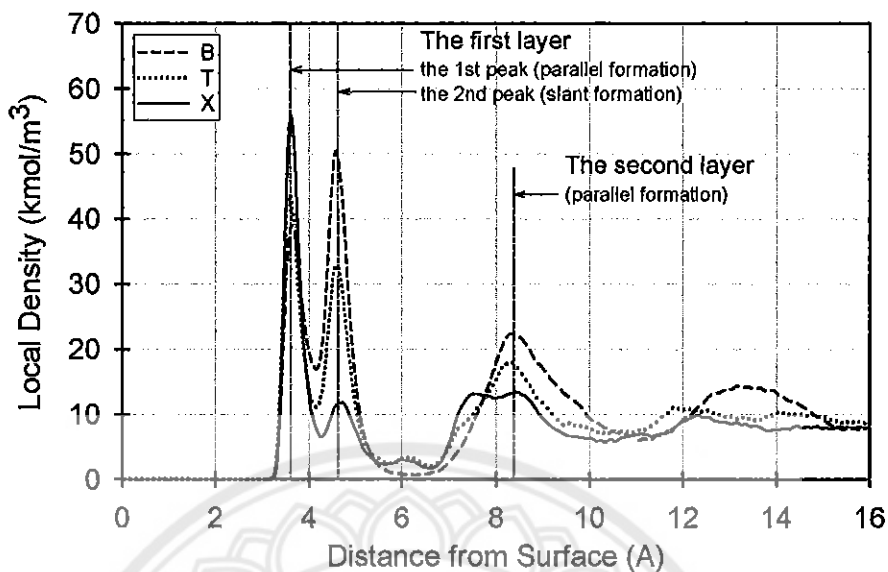
Figure 3.4 Local density distributions as a function of distance from a graphite surface to the centre of a benzene ring in BTX at 298K and a loading of 20µmol/m².

3.2 Polar aromatic hydrocarbons on graphitized surface

We now express our work on the adsorption of a polar aromatic, pyridine. Figures 3.5a and 3.5b show the adsorption isosterms and isosteric heats, respectively, of pyridine and BT on GTCB at 293K obtained from GCMC and the experimental data from the literature [5, 6, 15]. It has been found that the simulated reasults of pyridine is in good agreement with the experimental data at monolayer coverage, but under estimated at multilayers converage. However, this is reansonably to describe the affinity and packing of pyridine on GTCB at first time.

Figure 3.5 (a) adsorption isotherms and (b) isosteric heats of pyridine together
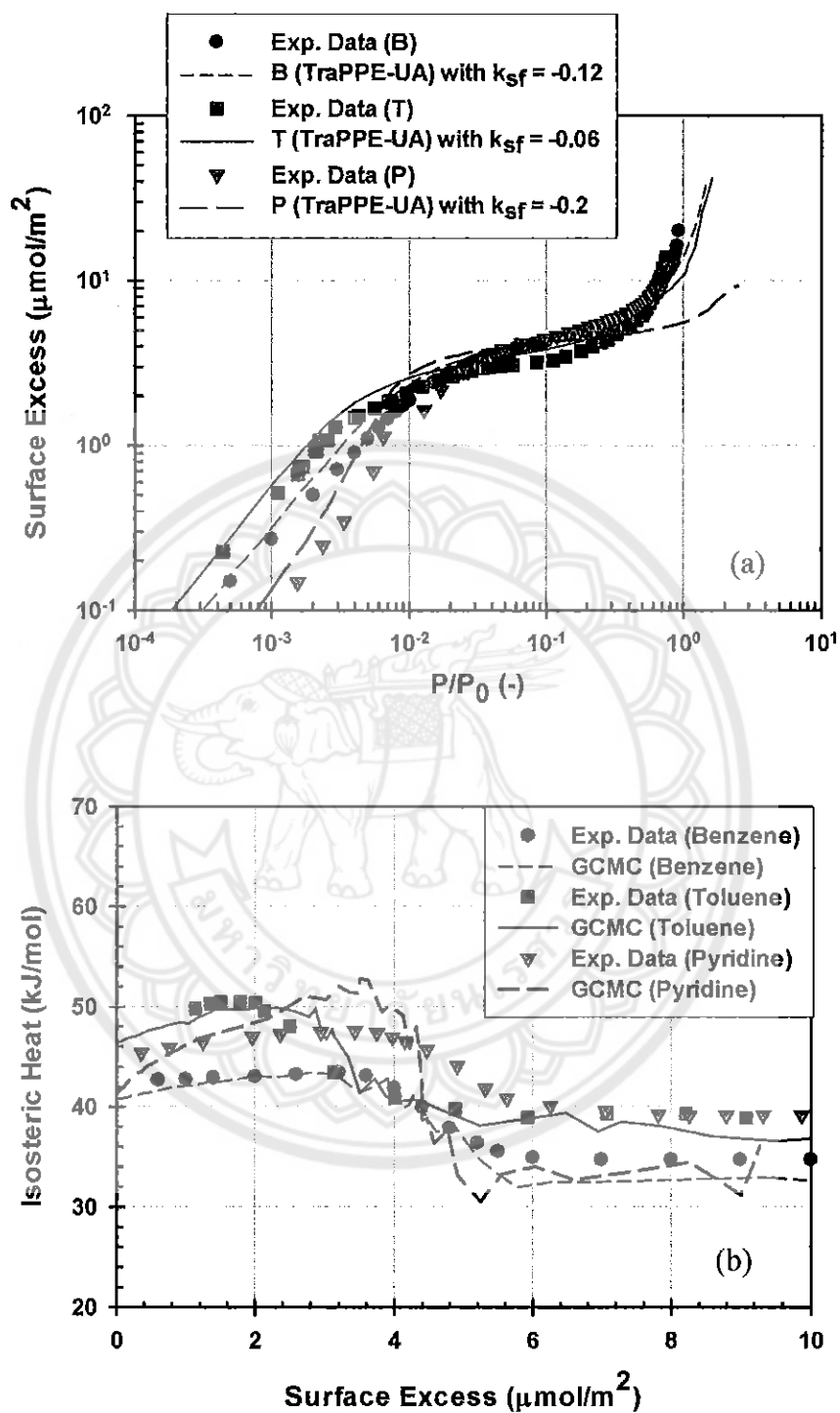with that of benzene and toluene on GTCB at 293K obtained with
GCMC and experimental data from the literature [5, 6, 15].

To see the contributions of the pyridine-solid and pyridine-pyridine interactions toward the isosteric heat, we plot these contributions in Figure 3.6 as a function of loading. In the sub-monolayer region, the increase in the pyridine-pyridine interactions compensates for the decrease in the pyridine-solid interaction, resulting in a relatively constant isosteric heat in this region. The pyridine-adsorbent interaction diminshes in the second layer because molecules are further away from the surface, while the adsorbate interaction increases only slightly giving a constant isosteric heat, of 37kJ/mol, compared to 50kJ/mol in the sub-monolayer region. The isosteric heat in the second layer of 37kJ/mol is close to the heat of liquefaction of pyridine, but this does not mean that the second layer is a liquid phase. The fluid-fluid interaction (FF) of the second layer is less than that in the bulk liquid because each molecule has fewer neighbours, and this is only partially compensated by the small fluid-solid interaction (FS). This is further supported when we study the structure of pyridine molecules in the next section.
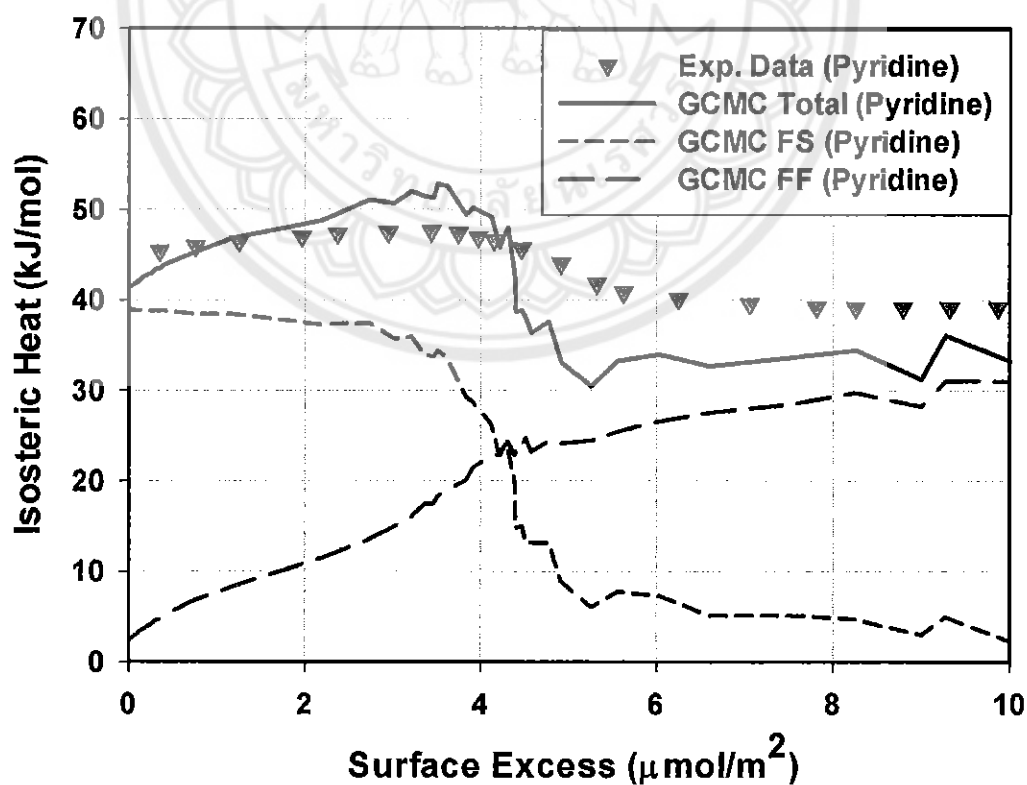

Figure 3.6 Isosteric heats of fluid-fluid and fluid-solid interactions for pyridine adsorption on GTCB at 293K obtained with GCMC.

Figures 3.7-3.10 show the local density distributions for the centre of mass of the ring with respect to the distance from the graphite surface at 293K.

First, we analyze the structure of pyridine molecules in the sub-monolayer region, and then later show how the presence of higher layers disturbs this structure because of the FF interactions from higher layers. The chosen isotherm points are shown in the inset of Figure 3.7, where A and B represent points well below the monolayer coverage and C and D are points just before and after the completion of the first layer. At points A and B, the surface is 15% and 50% covered with pyridine molecules, respectively. The first layer is about 3.7Å from the graphite surface which is slightly higher than that of BTX. At very low loadings there is a single peak indicating that all molecules have the same orientation parallel to the surface, as shown by snapshots in Figure 3.8a. However, at point C when the main peak of the first layer reaches the highest value a shoulder develops which then evolves into one minor peak in the local density distribution at point D (also see Figure 3.8b).
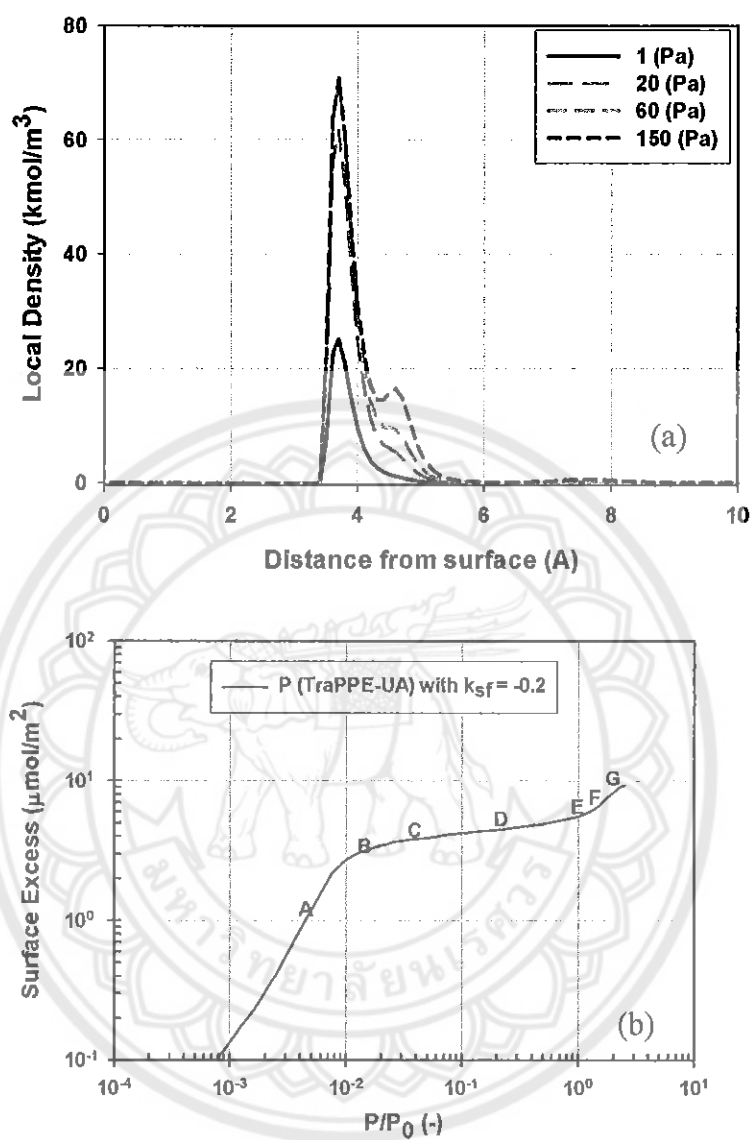
Figure 3.7 (a) Local density distributions of pyridine adsorption on GTCB at 293K obtained with GCMC at points A to D. (b) Points A to G are located on the corresponding isotherm.
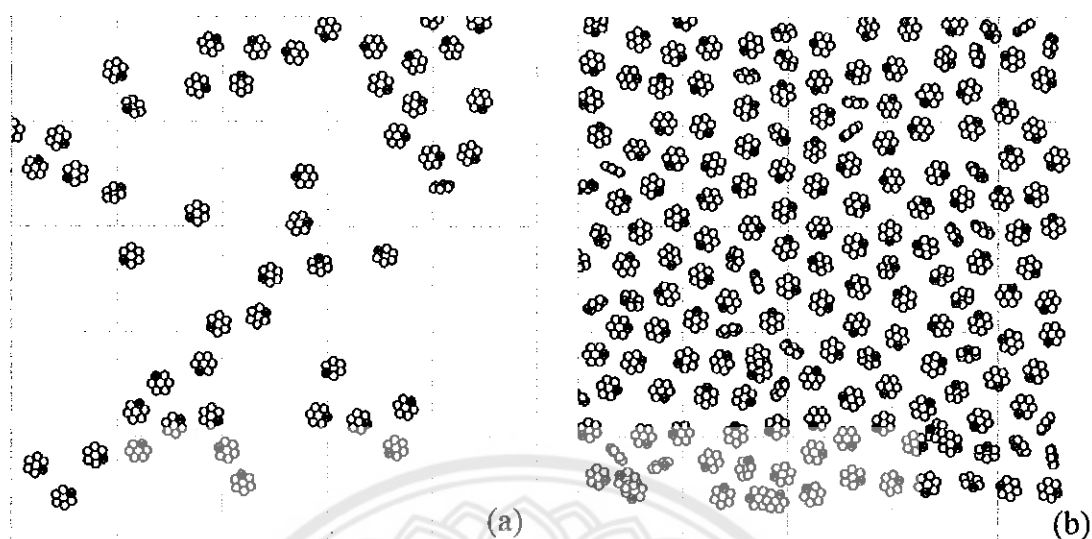
(a)   (b)

Figure 3.8 Top view of pyridine adsorption on GTCB at 293K obtained with
GCMC. (a) at Point A and (b) at Point D, where points **A and D** are
indicated in Figure 3.7.

These peaks do not result from the formation of another layer, but rather reflect the change in the orientation of some molecules, such that their centres of mass shift further away from the surface. These minor peaks are at 4.6Å which is slightly higher than that of BTX. The peak at 4.6Å is associated with molecules having a slant configuration. This configuration is not energetically favoured by the adsorbate-adsorbent interaction, but are favoured by the increase in the fluid-fluid interaction energy by having more molecules closer to the surface. However, it can be seen that the majority of molecules in the first layer remain parallel to the surface because the area under the first peak at 3.7Å is still the largest.

It is also interesting to observe that the minor peaks become higher when the second layer starts to form, i.e. more pyridine molecules in the first layer then adopt the slant and vertical configurations with the increase in the concentration of the second layer although the majority still remain in the parallel orientation.
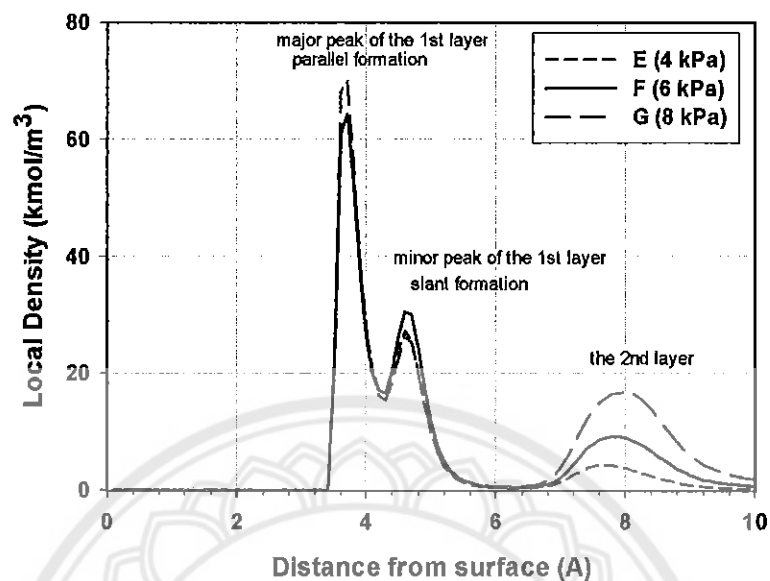
Figure 3.9 **Local density distributions of pyridine adsorption on GTCB at 293K obtained with GCMC at points E to G. Points E to G are indicated in Figure 3.7b.**

We provide more evidence for the moinor peak of the first layer in Figure 3.10 where the center of the ring and the center of N atom of pyridine are carried out to evaluate the local density distributions. We found that the minor peak is associated with the slant configuration where the N atom of pyridine is far away from the surface.
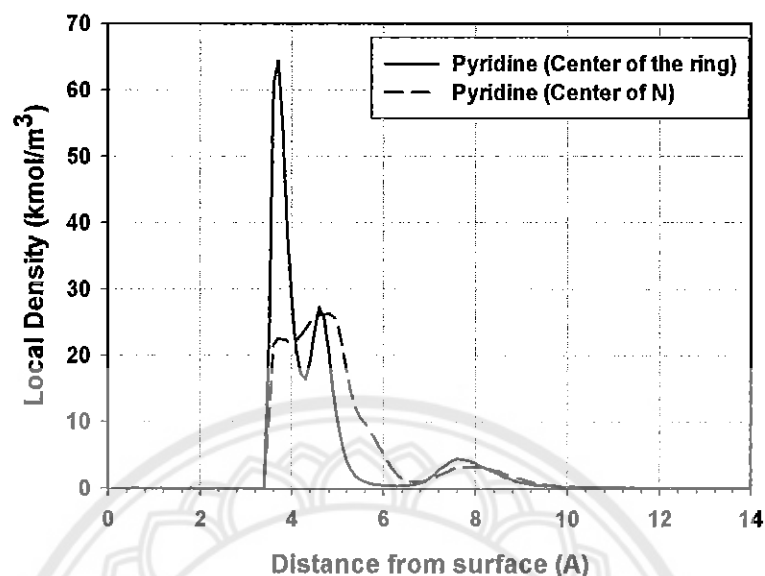
Figure 3.10 Local density distributions of pyridine adsorption on **GTCB at 293K** obtained with **GCMC** at points **E** where the centers are **at the center** of the ring and N atom of pyridine.

When the loading increases from the onset of the first layer to the second layer (points D to G in the inset of Figure 3.7b), the positions of the major and two minor peaks of the first layer are unchanged, but the peak position of the second layer moves from 7 to 8Å and becomes more delocalised. This is due to the presence of third layer, coupled with the thermal motion of molecules in the second layer. At point G, we note that although the positions of the minor peaks of the first layer do not change, the density of the major peak of the first layer is increased at the expense of the minor peaks, indicating that some molecules re-orientate themselves to the energetically favoured parallel configuration. This also maximises the quadrupolar interaction if pyridine molecules lie in offset positions when higher layers are present.

To further test the pyridine of multilayer adsorption on GTCB at different temperatures from 273-323K, we carry out simulation with the same k_{sf} as 293K as shown in Figure 3.11. Due to the strong interaction (FF and FS) at lower temperatures the uptakes and heats are higher than that of higher temperatures, but there is no particular trend with temperature.
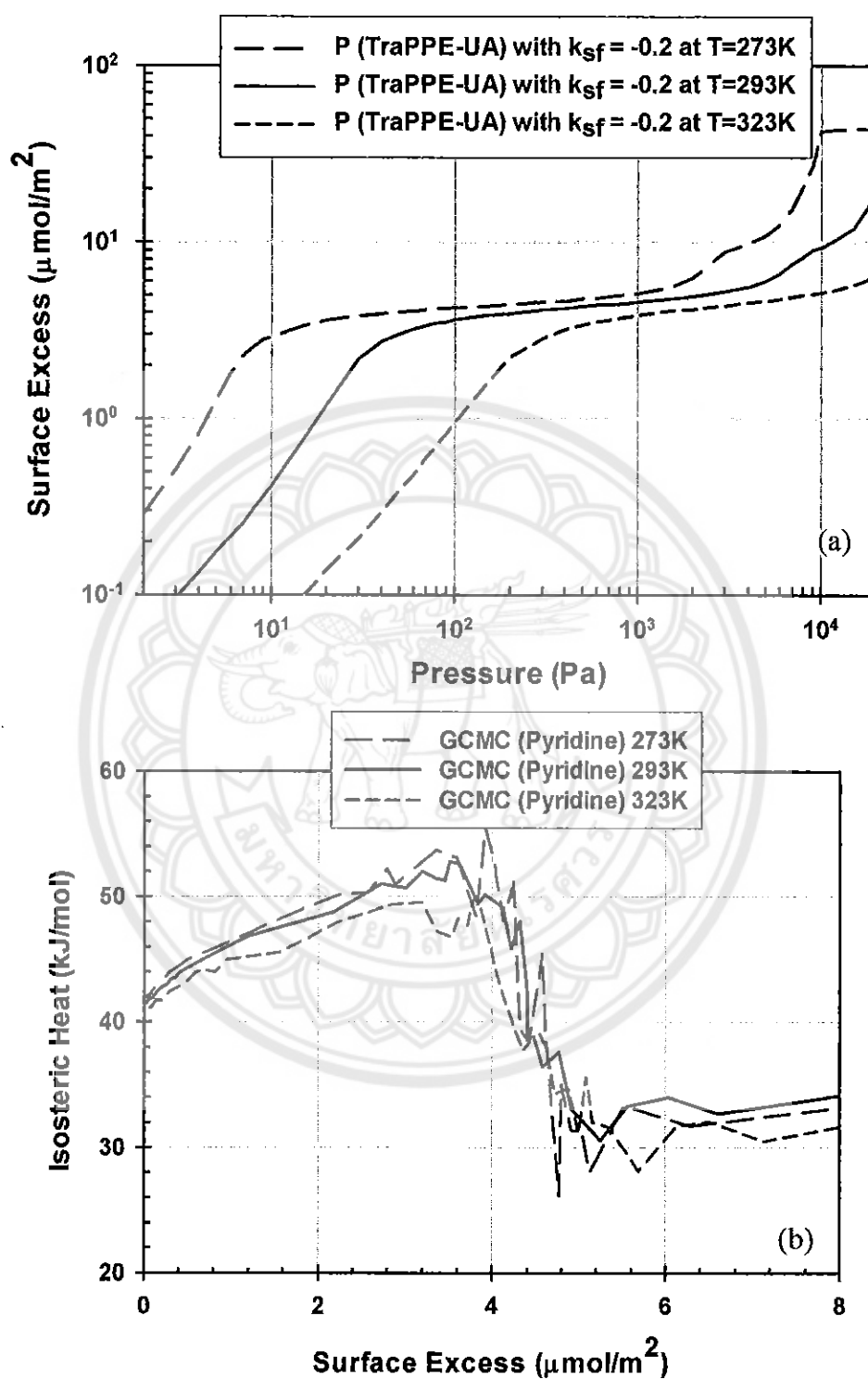
Figure 3.11 (a) Adsorption isotherms and (b) isosteric heats of pyridine on GTCB at different temperatures from 273 to 323K obtained with GCMC.
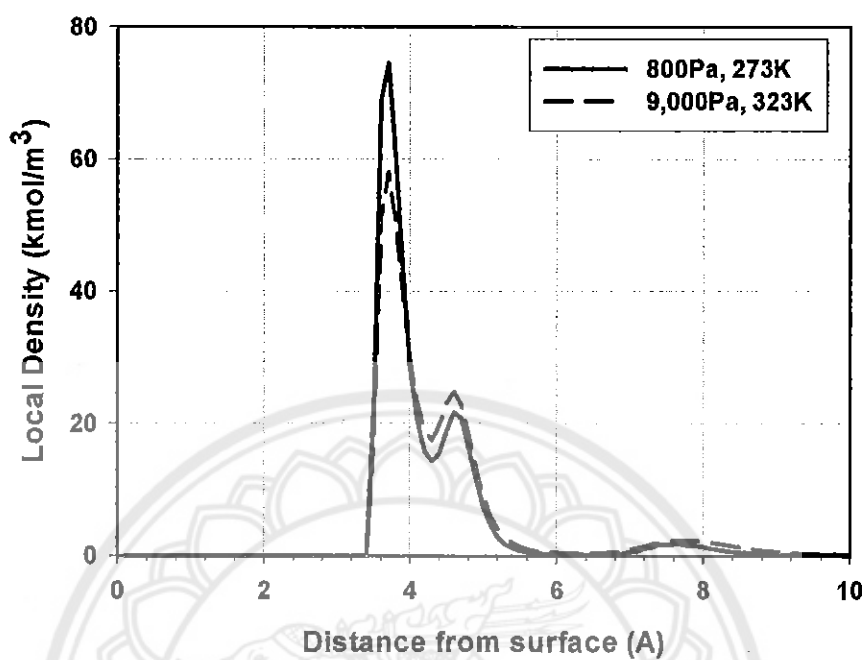
Figure 3.12 Local density distributions at just monolayer completed of pyridine on GTCB at 273 and 323K obtained with GCMC.
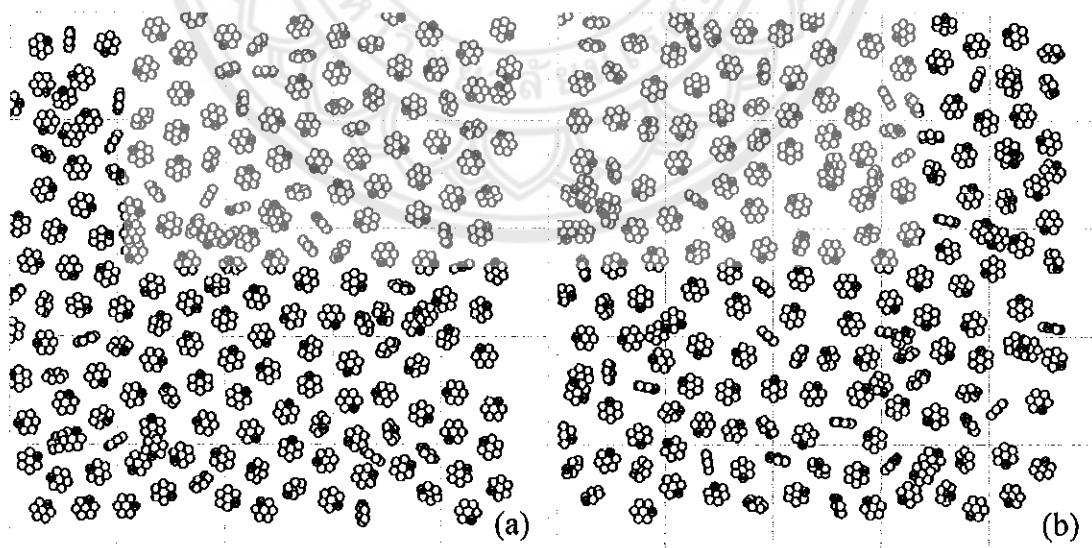
Figure 3.13 Snapshots of pyridine on GTCB at (a) 273K and (b) 323K where monolayer has just completed corresponding to Figure 3.12.

Finally, to illustrate the difference in the structure of the adsorbed film as temperature is increased, we show, in Figures 3.12 and 3.13 the local density distributions and the corresponding snapshots, respectively, for 273K and 323K. The structure of the first layer remains unchanged (although lower in density), but the structure of the minor peak of the first layer is higher due to the high thermal motion to minimize the energy of this minor peak with the multilayer. This observation is the same as BTX exception of the position of the peaks from the surface.

CHAPTER IV

CONCLUSIONS

4.1 Conclusions

We have presented computer simulations of adsorption non-polar and polar aromatic hydrocarbons on a graphite surface at ambient temperature. We have concluded by the following:

1. There are two peaks of the first layer where the main peak and minor peak are associated with the molecules having parallel and slant configurations, respectively.

2. The positions of the peak associated with molecules formation on graphite surface of BTX are not that different exception of their amount of adsorption.

3. Pyridine adsorption on graphite surface is similar to that of BTX. There are two peaks of the first layer but the position from the surface of pyridine of the first layer is slightly higher than that of BTX and the second peak of pyridine is closed to the surface rather than BTX.

REFERENCES

REFERENCES

1. White, R.F. and S.P. Proctor, *Solvents and neurotoxicity.* Lancet, 1997. **349**(9060): p. 1239-1243.

2. Ching-Mei Wang, Kuei-Sen Chang, and Tsair-Wang Chung, *Adsorption equilibria of aromatic compounds on activated carbon, silica gel, and 13X zeolite.* Journal of Chemical and Engineering Data, 2004. **49**(3): p. 527-531.

3. Ming-Hong Lai, Yi-Ling Shih, Yi-Hua Chen, Shih-Hong Shu and Tsair-Wang Chung, *Equilibrium Isotherms of the Adsorption of Pyrolysis Gases from Polymer Products.* Journal of Chemical and Engineering Data, 2010. **55**(2): p. 723-727.

4. Avgul, N.N., Berezin, G.I., Kiselev, A.V., Korolev, A.Ya., *Heat of adsorption of hydrocarbons by carbon blacks of different degrees of graphitization.* Kolloidnyi Zhurnal, 1958. **20**: p. 298-304.

5. N. N. Avgul, G. I. Berezin, A. V. Klselev, I. A. Lygina, *Heats of adsorption of toluene and various isoparaffins and naphthenes on graphitized carbon black.* Russian Chemical Bulletin, 1959. **8**(5): p. 764-773.

6. Isirikyan, A.A. and A.V. Kiselev, *The absolute adsorption isotherms of vapors of nitrogen, benzene and n-hexane, and the heats of adsorption of benzene and n-hexane on graphitized carbon blacks. I. Graphitized thermal blacks.* The Journal of Physical Chemistry, 1961. **65**(4): p. 601-607.

7. Isirikyan, A.A. and A.V. Kiselev, *Isotherms and Heats of Adsorption of Nitrogen, Benzene, and n-Hexane Vapours on Graphitised Carbon Blacks. III. Thermodynamic Quantities.* Russian Journal of Physical Chemistry, 1963. **37**(8): p. 957-961.

8. Davis, B.W. and C. Pierce, *A Study of Stepwise Adsorption.* The Journal of Physical Chemistry, 1966. **70**(4): p. 1051-1058.

9. Pierotti, R.A. and R.E. Smallwood, *The Adsorption of Benzene on Homogeneous Substrates.* Journal of Colloid and Interface Science, 1966. **22**(5): p. 469-481.

10. Pierce, C. and B. Ewing, *Localized Adsorption on Graphite Surfaces.* Journal of Physical Chemistry, 1967. **71**(11): p. 3408-3413.

11. Belyakov, L.D., A.V. Kiselev, and N.V. Kovaleva, *Gas-Chromotographic Determination of Isotherms and Heats of Adsorption of Water, Benzene and*

Methanol Vapours on Graphitised Carbon Black. Russian Journal of Physical Chemistry, 1968. **42**(9): p. 1204-1208.

12. Berezin, G.I., A.V. Kiselev, and V.A. Sinitsyn, *Adsorption of Benzene and n-Hexane on Graphitised Carbon Black.* Russian Journal of Physical Chemistry, 1970. **44**(3): p. 408-411.

13. G.I Berezin, A.V Kiselev, R.T Sagatelyan, V.A Sinitsyn, *A Thermodynamic Evaluation of the State of the Benzene and Ethanol on a Homogeneous Surface of a Nonspecific Adsorbent.* Journal of Colloid and Interface Science, 1972. **38**(2): p. 335-340.

14. P.J.M Carrott, M.M.L Ribeiro Carrott, I.P.P Cansado, J.M.V Nabais, *Reference data for the adsorption of benzene on carbon materials.* Carbon, 2000. **38**(3): p. 465-474.

15. Avgul, N.N., A.V. Kiselev, and I.A. Lygina, *Adsorption and heat of adsorption of pyridine and benzene vapor on graphitized carbon black.* Bulletin of the Academy of Sciences of the USSR, Division of chemical science, 1962. **11**(1): p. 26-30.

16. Vernov, A. and W.A. Steele, *Computer-Simulations of Benzene Adsorbed on Graphite.* Langmuir, 1991. **7**(12): p. 3110-3117.

17. Vernov, A. and W.A. Steele, *Computer-Simulations of Benzene Adsorbed on Graphite .2. 298-K.* Langmuir, 1991. **7**(11): p. 2817-2820.

18. Matties, M.A. and R. Hentschke, *Molecular dynamics simulation of benzene on graphite .1. Phase behavior of an adsorbed monolayer.* Langmuir, 1996. **12**(10): p. 2495-2500.

19. Matties, M.A. and R. Hentschke, *Molecular dynamics simulation of benzene on graphite .2. Phase behavior of adsorbed multilayers.* Langmuir, 1996. **12**(10): p. 2501-2504.

20. Do, D.D. and H.D. Do, *Adsorption of benzene on graphitized thermal carbon black: Reduction of the quadrupole moment in the adsorbed phase.* Langmuir, 2006. **22**(3): p. 1121-1128.

21. Yun, J.H., D.K. Choi, and S.H. Kim, *Equilibria and dynamics for mixed vapors of BTX in an activated carbon bed.* Aiche Journal, 1999. **45**(4): p. 751-760.

22. Masenelli-Varlot, K., E. McRae, and N. Dupont-Pavlovsky, *Comparative adsorption of simple molecules on carbon nanotubes - Dependence of the adsorption properties on the nanotube morphology.* Applied Surface Science, 2002. **196**(1-4): p. 209-215.

23. Artur P. Terzyk, Piotr A. Gauden, Sylwester Furmaniak, Radosław P. Wesołowski, Peter J. F. Harris and Piotr Kowalczyk, *Adsorption from aqueous solutions on opened carbon nanotubes-organic compounds speed up delivery of water from inside.* Physical Chemistry Chemical Physics, 2009. **11**(41): p. 9341-9345.

24. Morishige, K., *Freezing and Melting of Kr in Hexagonally Shaped Pores of Turbostratic Carbon: Lack of Hysteresis between Freezing and Melting.* Journal of Physical Chemistry C, 2011. **115**(6): p. 2720-2726.

25. Morishige, K., *Layer-by-Layer Freezing of Kr Confined in Hexagonal Pores with Crystalline Carbon Walls.* Journal of Physical Chemistry C, 2011. **115**(24): p. 12158-12162.

26. Yao Wang , Phuong T. M. Nguyen , Noriyuki Sakao , Toshihide Horikawa , D. D. Do ,Kunimitsu Morishige, and D. Nicholson , *Characterization of a New Solid Having Graphitic Hexagonal Pores with a GCMC Technique.* Journal of Physical Chemistry C, 2011. **115**(27): p. 13361-13372.

27. Wick, C.D., M.G. Martin, and J.I. Siepmann, *Transferable potentials for phase equilibria. 4. United-atom description of linear and branched alkenes and alkylbenzenes.* Journal of Physical Chemistry B, 2000. **104**(33): p. 8008-8016.

28. Wick CD, Siepman JI, Klotz WL, Schure MR., *Temperature effects on the retention of n-alkanes and arenes in helium-squalane gas-liquid chromatography - Experiment and molecular simulation.* Journal of Chromatography A, 2002. **954**(1-2): p. 181-190.

29. Jorgensen, W.L. and D.L. Severance, *Aromatic Aromatic Interactions - Free-Energy Profiles for The Benzene Dimer in Water, Chloroform, and Liquid Benzene.* Journal of the American Chemical Society, 1990. **112**(12): p. 4768-4774.

30. Rai, N. and J.I. Siepmann, *Transferable potentials for phase equilibria. 9. explicit hydrogen description of benzene and five-membered and six-membered*

heterocyclic aromatic compounds. Journal of Physical Chemistry B, 2007. **111**(36): p. 10790-10799.

31. Kiselev, A.V., D.P. Poshkus, and A.J. Grumadas, *Statistical Molecular Calculation of Thermodynamic Parameters os Adsorption of Aromatic-Hydrocarbons on Graphite .2. Polymethyl and Mono-Alkyl Benzenes.* Journal of the Chemical Society-Faraday Transactions I, 1979. **75**: p. 1288-1300.

32. Yun, J.H. and D.K. Choi, *Adsorption isotherms of benzene and methylbenzene vapors on activated carbon.* Journal of Chemical and Engineering Data, 1997. **42**(5): p. 894-896.

33. F. Haghseresht, J. J. Finnerty, S. Nouri, and G. Q. Lu, *Adsorption of aromatic compounds onto activated carbons: Effects of the orientation of the adsorbates.* Langmuir, 2002. **18**(16): p. 6193-6200.

34. Nikom Klomkliang, D.D. Do, D. Nicholson, C. Tangsathitkulchai, A. Wongkoblap, *Multilayer adsorption of benzene on graphitised thermal carbon black—The importance of quadrupole and explicit hydrogen in the potential model.* Chemical Engineering Science, (0).

35. Klomkliang, N., D.D. Do, and D. Nicholson, *Affinity and Packing of Benzene, Toluene, and p-Xylene Adsorption on a Graphitic Surface and in Pores.* Industrial & Engineering Chemistry Research, 2012. **51**(14): p. 5320-5329.

36. Wick CD, Stubbs JM, Rai N, Siepmann JI., *Transferable Potentials for Phase Equilibria. 7. Primary, Secondary, and Tertiary Amines, Nitroalkanes and Nitrobenzene, Nitriles, Amides, Pyridine, and Pyrimidine.* The Journal of Physical Chemistry B, 2005. **109**(40): p. 18974-18982.

37. Steele, W.A., *Physucal Interaction of gases with crystalline Solids .1. Gas-Solid Energies and Properties of Isolated Adsorbed Atoms.* Surface Science, 1973. **36**(1): p. 317-352.

38. Allen, M.P. and T.P. Tildesley, *Computer Simulation of Liquids.* Japanese Journal of Applied Physics Part 2-Letters, 1987. **35**(3B): p. L405-L407.

39. Ahmaruzzaman, M., *Adsorption of phenolic compounds on low-cost adsorbents: A review.* Advances in Colloid and Interface Science, 2008. **143**(1-2): p. 48-67.

40.   R.S. Araújo, D.C.S. Azevedoa, , , C.L. Cavalcante Jr.a, A. Jiménez-Lópezb, E. Rodríguez-Castellónb, *Adsorption of polycyclic aromatic hydrocarbons (PAHs) from isooctane solutions by mesoporous molecular sieves: Influence of the surface acidity.* Microporous and Mesoporous Materials, 2008. **108**(1-3): p. 213-222.

BIOGRAPHY

BIOGRAPHY

Name –Surname   Phitsanu   Sukniyom

Date of Birth   May 10, 1993

Place of Birth   Phitsanulok, Thailand

Address   30/100, Pralue Soi 3, Naimueang sub-district, Mueang

district, Phitsanulok, Thailand. 65000

Education Background

2014   B. Eng. (Chemical Engineering),

Naresuan University, Thailand

Name –Surname   Vutichai   Chaiyot

Date of Birth   May 4, 1993

Place of Birth   Kamphaengphet, Thailand

Address   24, 16 Alley, Tesaball Road, Naimueang sub-district,

Mueang district, Kamphaengphet, Thailand. 62000

Education Background

2014   B. Eng. (Chemical Engineering),

Naresuan University, Thailand